Lung CT Image Classification Algorithm Based on Improved Inception Network

Qianlan Liu
School of Information Engineering, Hunan University of Science and Engineering, Yongzhou, 425199, China

***Abstract*—With the continuous development of digital technology, traditional lung computed tomography medical image processing has problems such as complex images, small sample data, and similar symptoms between diseases. How to efficiently process lung computed tomography image classification has become a technical challenge. Based on this, the Inception algorithm is fused with the improved U-Net fully convolutional network to construct a lung computed tomography image classification algorithm model based on the improved Inception network. Subsequently, the Inception algorithm is compared with other algorithms for performance analysis. The results show that the proposed algorithm has the highest accuracy of 92.7% and the lowest error rate of 0.013%, which is superior to the comparison algorithm. In terms of recall comparison, the algorithm is approximately 0.121 and 0.213 higher than ResNet and GoogLeNct algorithms, respectively. In comparison with other models, the proposed model has a classification accuracy of 98.1% for viral pneumonia, with faster convergence speed and fewer required parameters. From this result, the proposed Inception network based lung computed tomography image classification algorithm model can efficiently process data information, provide technical support for lung computed tomography image classification, and thereby improve the accuracy of lung disease diagnosis.**

Keywords*—Image classification; inception; lung CT images; CNN; machine learning

I. Introduction

In recent years, the rapid development of medical technology has promoted the extensive application of computer-aided diagnosis system in the medical field, especially in the diagnosis of pulmonary diseases, where computer-aided system has shown great potential [1]. As a key link in the diagnosis of lung diseases, the accuracy of lung CT image classification directly affects the early detection and identification of diseases [2]. However, due to the complex structure and rich information of lung CT images, traditional classification methods are often difficult to effectively process, which not only limits the timely diagnosis of lung diseases, but also adversely affects the treatment effect and survival rate of patients [3]. In current studies, although deep learning has made many breakthrough achievements in the field of image classification, more refined and efficient algorithm models are still needed for specific challenges in lung CT image classification, such as high image complexity, limited sample data, and similar inter-disease symptoms [4-5]. Inception, as an important part of deep learning, can capture features of different levels through multiple branch networks and convolution nuclei of different scales, which provides the possibility to process the complex structure and rich information of lung CT images. Although the existing Inception network performs well in image classification, it still has some limitations when processing lung CT images. For example, the low degree of association between feature pixels and target pixels, as well as weak gradients of Inception module information, affect the accuracy and efficiency of classification. Therefore, this study aims to propose a lung CT image classification algorithm based on improved Inception network to enhance feature extraction and classification performance by fusing full convolutional networks (such as U-Net) to solve the problems encountered by existing algorithms in processing lung CT images. Compared with the existing research, the innovation point of this research is to integrate the improved Inception network with the full convolutional network, solve the problem of low correlation between feature pixels and target pixels by optimizing the structure of the convolutional layer and the pooling layer, and propose the combination of ResNet module and Inception module. To solve the problem of weak information gradient of Inception module. These improvements make the algorithm proposed in this study better than the existing algorithms, such as ResNet and GoogLeNet.

The research is divided into four parts. The first part analyzes the current research status of Inception algorithm and lung CT image classification models. The second part describes Inception and the CT image classification model constructed after fusion with a fully convolutional network. The third part analyzes the performance of the improved Inception algorithm and the improved Inception lung CT image classification model. The last part is a summary of the research.

II. Related Works

Imaging diagnosis of pneumonia remains a major medical challenge. Pneumonia is closely related to human life safety. The prevention and diagnosis of pneumonia are extremely important. The emergence and application of artificial intelligence provide technical support for the treatment of lung diseases. Kocks et al. proposed a machine learning algorithm tool for the diagnosis of asthma, COPD, and overlapping conditions, and compared it with primary care physicians and pulmonary specialists. The results show that the algorithm tool has excellent diagnostic performance and provides strong support for the identification of pulmonary diseases [6]. To solve the problem of inaccurate prediction of lung diseases, Annamalai's team proposed a convolutional neural network based on auction optimization algorithm. The results show that this method is superior to traditional methods in predicting performance and provides a new idea for the early diagnosis

of lung diseases [7]. Wobma et al. developed a screening algorithm for lung disease screening in patients with systemic juvenile idiopathic arthritis. The results show that the algorithm can effectively identify lung diseases in patients and improve the accuracy and efficiency of screening [8]. Zhang et al. reviewed machine learning applications for chronic obstructive pulmonary disease. The results show that machine learning has a broad application prospect in the diagnosis, treatment and management of this disease, providing strong support for clinical decision-making [9]. In order to improve the accuracy of inference for chronic obstructive pulmonary disease, Cosentino et al. proposed a deep learning model based on the original respiratory map. The results show that this method can identify new genetic loci and improve the risk model, providing a new way for the precision medicine of diseases [10].

With the improvement of medical data resources and the development of auxiliary diagnosis and treatment methods for lung diseases, lung CT medical imaging technology plays a crucial role in clinical medicine and lung disease screening. An accurate image classification model can improve the utilization rate of medical resources. To address the shortcomings of training data and its inter class similarity and variability in chest CT scans, Wang et al. proposed a two-stage deep learning strategy. It is used for invasive classification of solid nodules in chest CT images. The results show that the accuracy of the proposed binary classifier is 83.4% ± 1.4, and the AUC is 91.3% ± 2 [11]. To explore the imaging characteristics of congenital tracheal stenosis combined with left pulmonary artery suspension surgery, Fukushima team proposed a qualitative variable model based on clinical features and computed tomography imaging. After testing the model, it was found that 38 cases (86%) of bilateral lung patients has left pulmonary artery suspension surgery [12]. To determine the overall positive rate of pulmonary arteriography and the factors that affect the results of pulmonary arteriography, Aggarwal et al. conducted experiments using methods such as logistic regression analysis. The results showed that the pulmonary angiography rate in the study was 10.9%, higher than the study results with a positive rate of<2% [13]. To explore the role of preoperative CT examination results in predicting acute postoperative exacerbation in patients with gestational pneumonia and cancer, Ozawa et al. used Fisher exact test and Mann-Whitney U test. The test results show that common patterns of gestational pneumonia show 58% acute exacerbation and 73% no acute exacerbation [14]. To accurately estimate the volume of pulmonary nodules and reduce the workload of doctors, Lee proposed an intelligent method for automatically detecting and segmenting pulmonary nodules from computer tomography. The results show that the average and standard deviation of the segmentation overlap measure are 0.81 and 0.08, respectively [15].

In summary, artificial intelligence is applied to all aspects of society. In the era of data and information, people are increasingly reliant on deep neural networks. The improved concept network model is widely used in various fields such as biological component detection, adaptive learning models, and biological gene networks. With the increasing attention paid to lung health, more experts and scholars have conducted experimental research to find the optimal lung CT image classification model. However, lung CT image classification models based on improved Inception have been rarely studied. To make up for this deficiency, a lung CT image classification algorithm model based on an improved Inception network is constructed, thereby promoting the organic integration of artificial intelligence and medicine.

III. Construction of an Improved Inceptional Lung CT Image Classification Model

Nowadays, the application of artificial intelligence in medical images is also gradually increasing. Among them, convolutional neural networks have made significant contributions to medical image processing [16]. The algorithm network based on Inception can obtain deeper level data from medical images, improving the accuracy of image judgment.

A. Construction of a Lung CT Image Classification Model based on Traditional Inception

To integrate the Inception module, convolutional layers and pooling layers are fused together. The pooling layer mainly involves repairing feature images to enhance the correlation between feature pixels and target pixels [17]. This method can effectively save the central and surrounding features of the feature image, avoiding problems such as traditional maximum or average pools ignoring partial feature information [18]. The traditional maximum pooling operation is shown in Fig. 1.

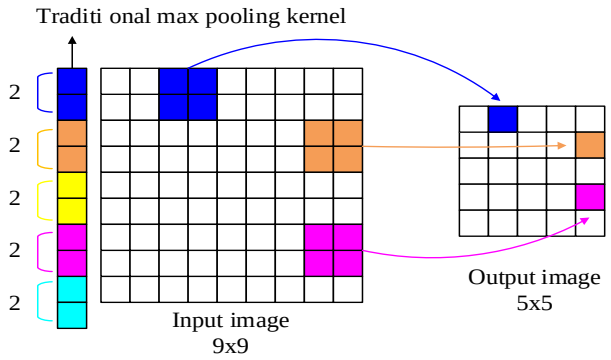

Fig. 1. Traditional maximum pooling operation.

Fig. 1 shows the traditional maximum pooling operation. The left side of Fig. 1 shows the input image. The right side shows the output image. The input image usually has a 9x9 pool core. The pool core size is uniform and fixed in distribution. The output image usually has a 5x5 pool core. The distribution of the output pool cores is uniform. The purpose of pooling layers is to reduce the dimensionality of convolutional layers and reduce the parameters during operation. Afterwards, residual modules and skip connections are used to increase the number of network layers. The calculation of the residual network is shown in Eq. (1).

$$F(x_1) = w \cdot x_1 + b \tag{1}$$

In Eq. (1), x_1 is the input value. w is the weight. b is offset. After the learning signal of the neuron is transmitted to other neurons, the activation function is used to calculate the

sum of the two branch layers. The input data is subjected to data transformation. The activation function is shown in Eq. (2).

$$y_1 = R(F) + h(x_1) \tag{2}$$

In Eq. (2), y_1 represents the input data transformation. y_1 is the sum of two branch layers. After data input and activation, perform residual module output, and the residual module output formula is shown in Eq. (3). It can effectively accelerate training speed and improve the accuracy of parameter adjustment.

$$x_{l+1} = R(y_1) \tag{3}$$

In Eq. (3), x_{l+1} is the output of the residual module. To prevent problems such as gradient dispersion, activation function is used. To enhance the propagation speed of the function, ReLU activation function is used to reduce gradient attenuation caused by deep convolution. The formula for ReLU is shown in Eq. (4).

$$R(x) = \max(0, x) \tag{4}$$

According to Eq. (4), when $x > 0$, $R(x) = x$, the derivative is 1. When $x < 0$, $R(x) = 0$, the derivative is 0. Traditional pooling cannot automatically adapt to changes in the specific location of pooling. Therefore, the Inception module adopts central pooling to preserve the central features of the patch. The central pooling operation process is shown in Fig. 2.

Fig. 2 shows the operation process of central pooling. A large pool core and a small pool core are designed in the central pool structure. The image center selects a small pool core. The image edge adopts a large pool core. This structure can eliminate many edge features. The operation steps first define the pooling area. Pooling operations are typically performed within a certain area of input data. The defined indicators are the size and shape of the area. Rectangles and circles are usually common shape features. Secondly, the total pooling value is calculated. Based on the specific pooling type, a pooling value is calculated within the pooling area. Common pooling types include maximum pooling, average pooling, and L2 pooling. Next, the summary value is output, which represents the information within the pooled area. Finally, the pooling window is moved. The pooling window is moved to the next position of input data. Afterwards, the above steps are repeated until they cover the entire input data. After the operation is completed, in order to avoid information loss during repeated down sampling and up sampling, a fusion multi-convolutional layer feature method is adopted to increase the flow ability of the data image. The specific operation is shown in Fig. 3.

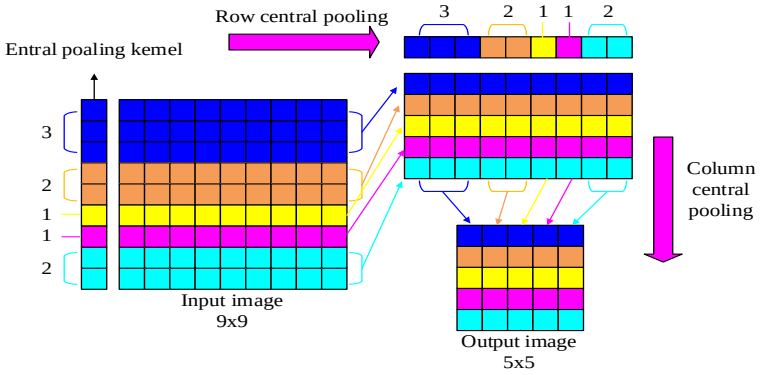

Fig. 2. Central pooling operation.

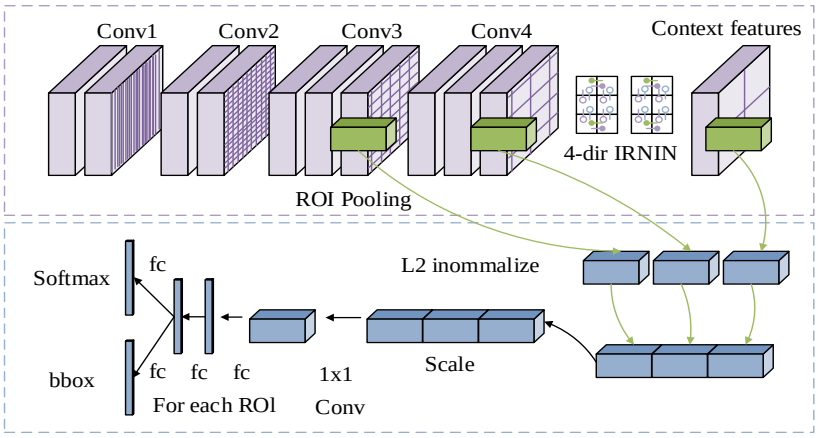

Fig. 3. Inside-outside network.

Fig. 3 shows the inner and outer network structure of the shallow convolutional layer in the Inception module using feature maps. Fig. 3 fuses multiple convolutional layers. The upper and lower features in the image are extracted and normalized in the ROI pool. After the Inception network collects features from the input image in parallel, multiple such Inception modules are first connected in series. Afterwards, all output results are concatenated into feature maps. Different sizes of convolutional kernels are beneficial for diversified feature extraction. The method of collecting signal features in parallel can effectively increase the width of the network and the adaptability to scale. This can effectively reduce information loss caused during the data sampling process, which is more conducive to machine learning.

B. *Construction of an Improved Inception Lung CT Image Classification Model*

The Inception module has four generations, namely the original version, Inception-v1, Inception-v2/v3, and Inception-v4. During the iteration process, the performance of Inception is gradually improved [19]. The traditional Inception model requires a large amount of computation. The information gradient of network backpropagation is weak. On this basis, the Inception model is improved [20-21]. Because ResNet can introduce residual connections, the network can directly transfer the features of the front layer to the back layer, thus effectively alleviating the problem of gradient disappearance. Moreover, it can enhance the feature extraction ability of the network by transmitting feature information directly. In the classification of lung CT images, the accuracy and diversity of feature extraction are very important to improve the classification performance. ResNet's structural design allows the network to more efficiently capture features at different levels in the image, which is very helpful for distinguishing subtle lung lesions. Therefore, the improved method proposed in this study is to integrate Inception with ResNet for better image classification and target detection. The improvement method is to fuse Inception with ResNet for better classification, object detection, and image segmentation. Then the corresponding information of Inception and ResNet module is overlaid. The specific algorithm is shown in Eq. (5).

$$M = \sigma(C_2\theta(C_1 \cdot x)) \tag{5}$$

In equation (5), M represents the output function. σ represents a nonlinear layer. C_2 is the scaling parameter. θ represents the activation function value. x represents the output result. In classification calculations, the loss function is used to standardize two probability distributions a and b. Then b is used to describe a. The cross entropy formula is shown in Eq. (6).

$$H(a,b) = -\sum a(x)\log b(x) \tag{6}$$

$H(a,b)$ represents the cross entropy value. $a(x)$ represents the probability distribution. $\log b(x)$ represents the probability distribution of b. Cross entropy, as a measure of the similarity between two probability distributions, is widely used in machine learning. It is mainly used to measure the difference between the predicted output of the model and the actual output. In Eq. (7), the cross entropy satisfies the probability distribution function.

$$\forall xa(X-x) \in [0,1] and \sum a(X-x) = 1 \tag{7}$$

In Eq. (7), X is the true value predicted by the model. b is the output value predicted by the model. $a(X-x)$ is the distribution function. Eq. (7) indicates that the probability of events occurring is between 1, and 0. The sum of probabilities is always 1. The improved Inception module is mainly divided into six steps to complete. The schematic diagram of the model is shown in Fig. 4.

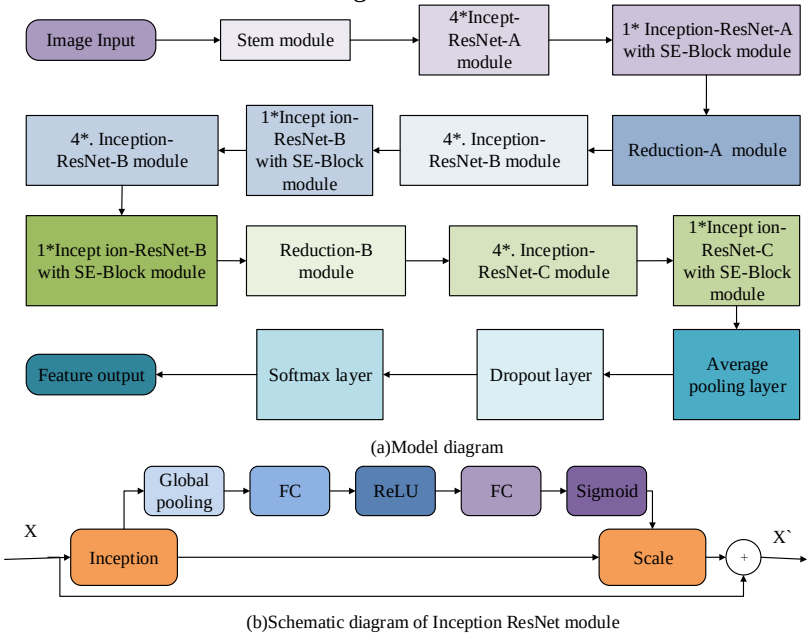

Fig. 4. Module diagram

Fig. 4(a) is a schematic diagram of the convolutional neural network architecture. Fig. 4(b) is a schematic diagram of the Inception ResNet module. Inception and ResNet network structures are combined, and sections such as Stem, SE-Block, and Reduction are added to them. To increase the running speed and deepen the network depth, the convolution size is changed in the model. The residual structures are introduced to solve the overfitting problem. Then, feature weights are added and activation functions are replaced. Finally, the number of classifications is determined. To achieve high network convergence speed in model training, all convolutional layers and inner product activation layers are used in the original U-Net network structure. The normalization formula used is shown in Eq. (8).

$$H_{ab}^{c} = \frac{H_{ab}^{c} - \mu_{ab}}{\sigma_{ab}} \tag{8}$$

In Eq. (8), σ_{ab} represents the output when a neurons in the b layer are trained to c data. μ_{ab} is the average output of a neurons in layer b. σ_{ab} represents the standard deviation of a neurons in layer b. The average output of neurons is shown in Eq. (9).

$$\mu_{ab} = \frac{1}{d}\sum_{c=1}^{d} H_{ab}^{c} \tag{9}$$

In Eq. (9), μ_{ab} is the average output of a neurons in the b layer. σ_{ab} represents the output when a neurons in layer b are trained to c data. $\frac{1}{d}$ represents the mean after summing σ_{ab}. After obtaining the mean formula of the neuron, the standard deviation of the neuron output is calculated. The standard deviation formula is shown in Eq. (10).

$$\sigma_{ab} = \sqrt{\sigma + \frac{1}{d}\sum_{c=1}^{d}(H_{ab}^{c} - \mu_{ab})^{2}} \tag{10}$$

In Eq. (10), σ_{ab} is the standard deviation of a neurons in layer b. μ_{ab} is the average output of a neurons in layer b. The values of σ and d are constants. The specification layer is placed before the activation function. The activation function of the specification layer is normalized in batches, as shown in Eq. (11).

$$y = f(BN(\sum_{a} W_a X_a)) \tag{11}$$

y represents the normalization function. $W_a X_a$ represents the connection degree between input neurons and output neurons. The bias parameter b is normalized by the system after passing through the specification layer. The main task of the BN layer is to normalize the input data values of neurons. The output values are unified within the interval of [0,1] to improve model accuracy. After building the model, the system development environment is built. In the pneumonia classification system, the B/S architecture is selected. The specific system architecture diagram is shown in Fig. 5.

Fig. 5 shows the UML sequence diagram of the pneumonia classification and prediction module. The system page includes two aspects, namely "Select File" and "Forecast". Users can click and select the corresponding test chart in the "Select File" section. The situation where there are a large number of categories in lung CT images that cannot provide classification entry points for each category can be avoided. Afterwards, the "Forecast" button is clicked to perform prediction analysis. When the user enters the platform homepage, the predicted results can be obtained. The controller calls the query interface of the experimental model to obtain CT images. The view layer posts the transmitted information on the page. Finally, the predicted results of pneumonia CT images are obtained. The corresponding probability sizes of the results are displayed in the interface. The graph cutting algorithm is used in the image, which locks and marks the target of the image. The formula is shown in Eq. (12).

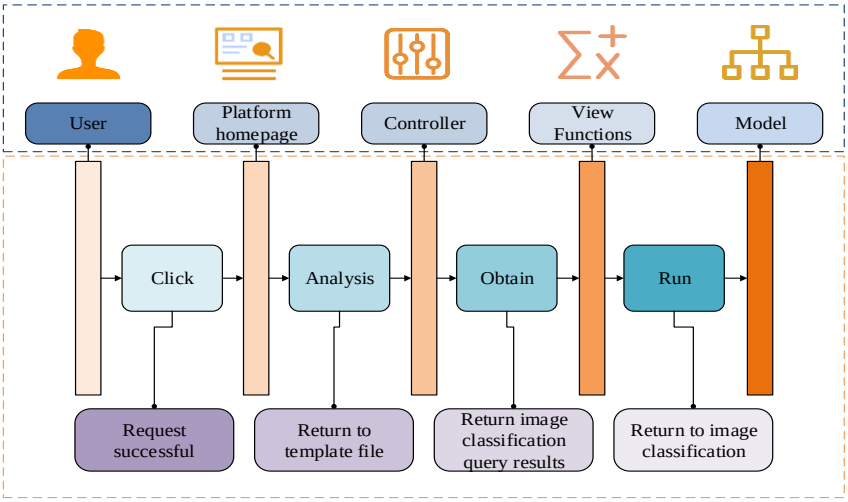

Fig. 5. UML sequence diagram of pneumonia classification and prediction module.

$$E(A) = \lambda R(A) + B(A) \tag{12}$$

In Eq. (12), A represents pixels. B represents the background pixel. $E(A)$ is the energy function. λ is the influence coefficient of the regional energy function on the total energy function. The energy function of the region term is shown in Eq. (13).

$$R(A) = \sum R_P(A_P) \tag{13}$$

In Eq. (13), $R(A)$ represents the regional energy function. R_P represents the probability of the target area. A_P represents the division of pixels. Next, the pixels are labeled as background points and front attractions. The formal expression of $R_P(A_P)$ is shown in Eq. (14).

$$R_p(O) = -\ln \Pr(I_P / O) \tag{14}$$

In Eq. (14), $\Pr$ is the target probability. R_p is the probability result. O represents the pixel of the image. After the "prediction" button is clicked, corresponding prediction analysis is performed, and then the experimental model is called using the controller. After the calculation is completed, the prediction results of the pneumonia CT image are displayed in the front interface. In summary, traditional Inception networks have low classification efficiency. It is not conducive to saving medical resources. Based on this, the traditional Inception network is improved. The improved U-Net full convolutional network image semantic segmentation is integrated into the model to improve the convergence speed of the network. This solves the segmentation speed, laying the foundation for building the optimal lung CT image classification algorithm model.

IV. Evaluation of Lung CT Image Classification Algorithm Based on Improved Inception Network

The improved Inception network lung CT image classification algorithm model can effectively enhance the accuracy of image classification. Compared to other models, the classification performance and fitting degree are superior. It requires fewer parameters. Building a system model framework on the improved U-Net is beneficial for enhancing the sensitivity of image segmentation and making the lung structure clearer.

A. Parameters Design and Evaluation of Improved Inception Network

To avoid inconsistent size and singularity in the lung CT dataset, a pneumonia CT database is constructed for abnormal pneumonia, viral pneumonia, and normal images. The specific content is shown in Table I.

TABLE I. Database

Classification	Normal CT images	Normal CT images	Abnormal CT images
Total	2300	2200	2300
Training set	1500	1300	1600
Validation set	500	500	500
Test set	600	600	600

Table I shows the pneumonia CT database constructed during this training. A total of 6800 pneumonia CT images are selected, including 4400 for training, 1500 for validation, and 1800 for testing. After preprocessing the data, 4400CT images are selected for training. The classification results of ResNet, GoogLeNct, and Inception ResNet are compared. The results are shown in Fig. 6.

Fig. 6 shows the recall rate of the classification results of the three algorithms in CP. The recall rates of ResNet, GoogLeNct, and Inception-ResNet in CP are 0.812, 0.701, and 0.953, respectively. In NCP, the recall results of the three algorithms are 0.754, 0.635, and 0.981, respectively. In the recall rate results of Normal, the Inception-ResNet algorithm is 0.121 and 0.213 higher than ResNet and GoogLeNct algorithms, respectively. From this, it can be seen that the Inception ResNet algorithm in this research has the highest recall rate in CP, NCP, and Normal. Therefore, it has the most superiority. Then, the error and specificity of the three algorithms are compared and analyzed. The results are shown in Fig. 7.

Fig. 7 shows the comparison results of error rates and specificity among the three calculations. Fig. 7(a) shows the comparison results of error rates among the three algorithms. In CP, the training error of Inception-ResNet is 0.013%, the error rate of GoogLeNct is 0.034%, and the error rate of ResNet is 0.023%. In NCP, the error rates of Inception-ResNet are 0.012% and 0.021% lower than those of ResNet and GoogLeNct algorithms. In Normal, the error rates of Inception-ResNet are 0.014% and 0.022% lower than those of ResNet and GoogLeNct algorithms. From this, the Inception-ResNet algorithm in this research has a smaller error rate compared to the other two algorithms. In Fig. 7(b), the Inception-ResNet in CP is 90.1%, which is about 31% and 42% higher than ResNet and GoogLeNct. In NCP, it is about 29.8% and 36.2% higher than ResNet and GoogLeNct. In Normal, it is about 31.2% and 34.3% higher than ResNet and GoogLeNct. From this, the Inception-ResNet algorithm has better classification performance. To further analyze the segmentation performance of Inception-ResNet algorithm in pneumonia CT images, CNN, FCN, GraphCut, region growth value, adaptive threshold and other algorithms are selected for comparison. The results are shown in Fig. 8.

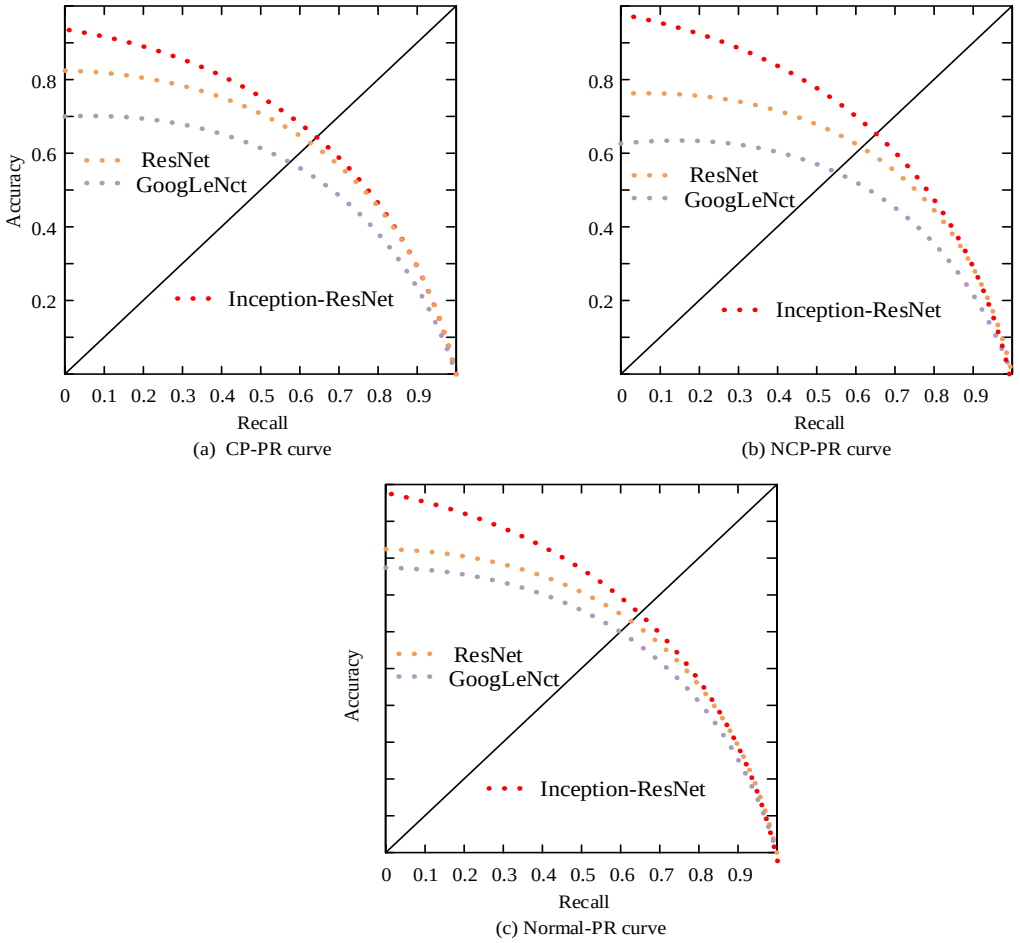

Fig. 6. Recall three algorithms.

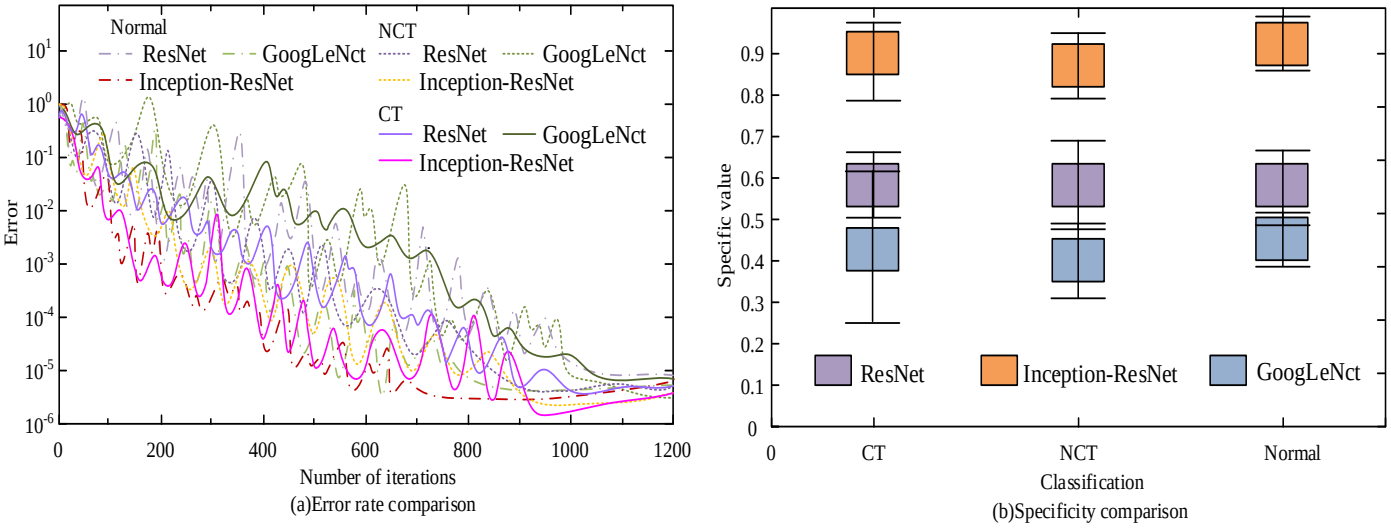

Fig. 7. Comparison of error and specificity.

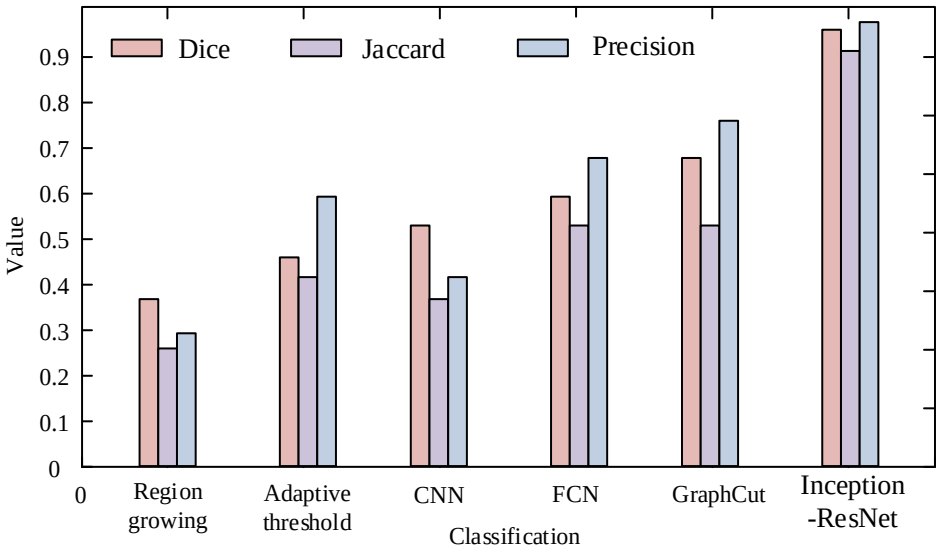

Fig. 8. Algorithm comparison histogram

Fig. 8 shows the comparison between the Inception-ResNet algorithm and other algorithms. Compared to other algorithms, Inception-ResNet algorithm has a leading advantage in segmentation accuracy. In the comparison of Dice coefficient and Jaccard coefficient, the Inception-ResNet algorithm is about 0.25 and 0.29 higher than other algorithms, respectively. The Dice coefficient, Jaccard coefficient, and accuracy are the lowest in regional growth. The Dice coefficient, Jaccard coefficient, and accuracy values of the CNN algorithm are 0.51, 0.38, and 0.40, respectively. The Dice coefficient, Jaccard coefficient, and accuracy values of the FCN algorithm are 0.6, 0.54, and 0.68, respectively. The Dice coefficient, Jaccard coefficient, and accuracy values of the GraphCut algorithm are 0.69, 0.51, and 0.77, respectively. The Dice coefficient, Jaccard coefficient, and accuracy values of the Inception-ResNet algorithm are 0.93, 0.91, and 0.96, respectively, all exceeding 0.9. The Inception-ResNet algorithm converges faster, which is beneficial for the segmentation of lung images.

B. Performance Analysis of Improved Inception Network Model

To evaluate the segmentation effect of the improved Inception network model on pneumonia CT images, segmentation experiments are conducted on the model based on image segmentation techniques. During the experiment, the loss function curve was used to represent the iterated values, and the original U-Net is compared with the improved U-Net data. The results are shown in Fig. 9(a). Afterwards, segmentation is performed on different positions of the lungs to segment the main body of the lung CT image. The final result is shown in Fig. 9(b).

Fig. 9(a) shows the loss function of the network model. In model comparison, the convergence speed of the original network model is slower than the DB-U-Net Loss model proposed in the research. When the DB-U-Net Loss model is less than 0.1, the loss function converges rapidly and reaches a minimum value around 0.18. When the number of iterations is 20, it approaches 0. The original model approaches 0 at 45 iterations. The convergence speed is relatively slow. This indicates that the improved model has better network performance. Fig. 9(b) shows the segmentation results of pneumonia images. The improved model can accurately segment lesions with pneumonia features, which has a high degree of segmentation granularity. When the segmentation model reaches the optimal level, collect the operational status of pneumonia CT images within 48 hours. The average response time, fault condition, and waiting time for the slowest response of the system are used for data comparison. The analysis results of the model performance are shown in Fig. 10.

The white screen time and first screen time in Fig. 10 reflect the response speed of the system when processing CT images of pneumonia. The white screen time refers to the time from the user's request to the system's content display, and the first screen time refers to the time from the system's content display to the completion of the main page content loading. The length of these two times directly affects the user experience, and the shorter the time, the faster the system response and the better the user experience. Fig. 10 shows the performance analysis of the model system proposed in this study. As shown in the figure, the average first screen time in the pneumonia CT image classification system is 1.01s. The average white screen time is 0.81s. The average full screen time is 1.36s. The full screen time is the longest, approximately 0.35s and 0.55s higher than the average white screen time and average first screen time, respectively. As the iteration increases, the white screen time is the most stable. The overall screen time fluctuates significantly. The first screen time fluctuates greatly when the number of iterations is 2-30. This functional test shows that the performance of each functional module and page is normal. There is no malfunction in the reaction sensitivity, and the reaction force is sensitive. Finally, the analysis is conducted using a confusion matrix approach. ResNet and GooLeNet models are compared with the Inception-ResNet model for image classification accuracy. The results are shown in Fig. 11.

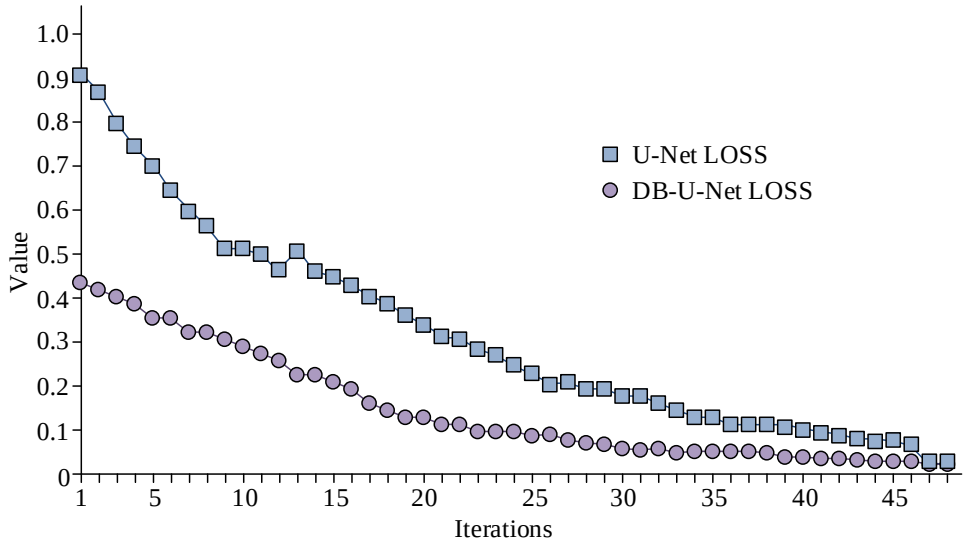

(a)Iterative Network Model Loss Function

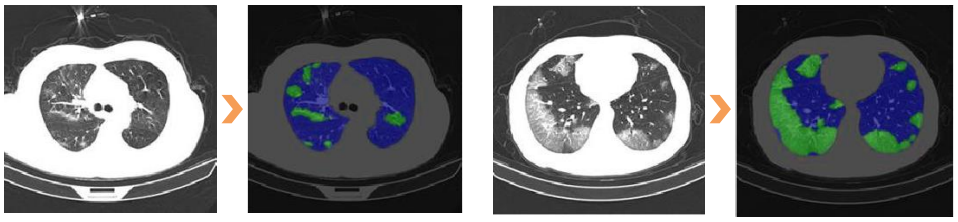

(b)Pneumonia image segmentation

Fig. 9. Loss function and image segmentation.

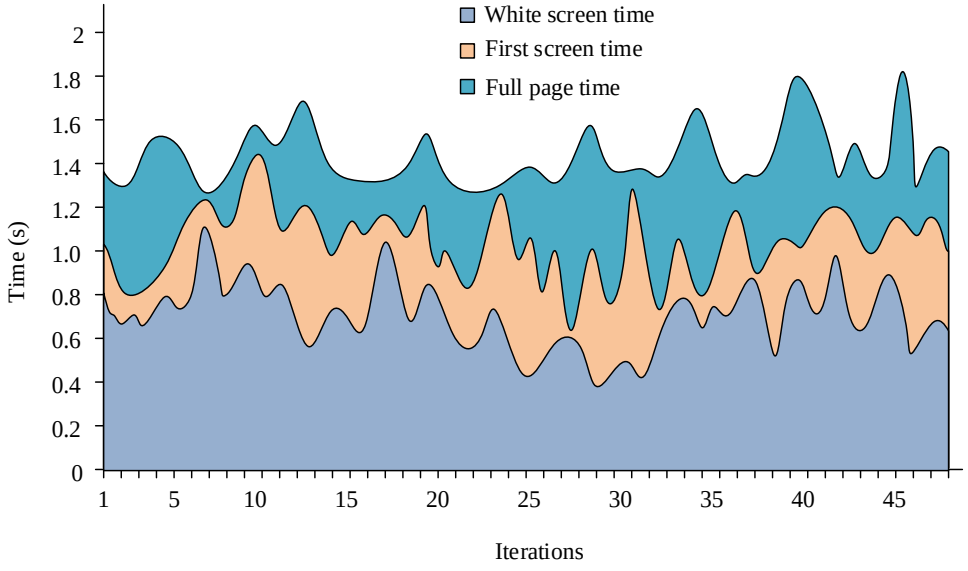

Fig. 10. Model system performance analysis.

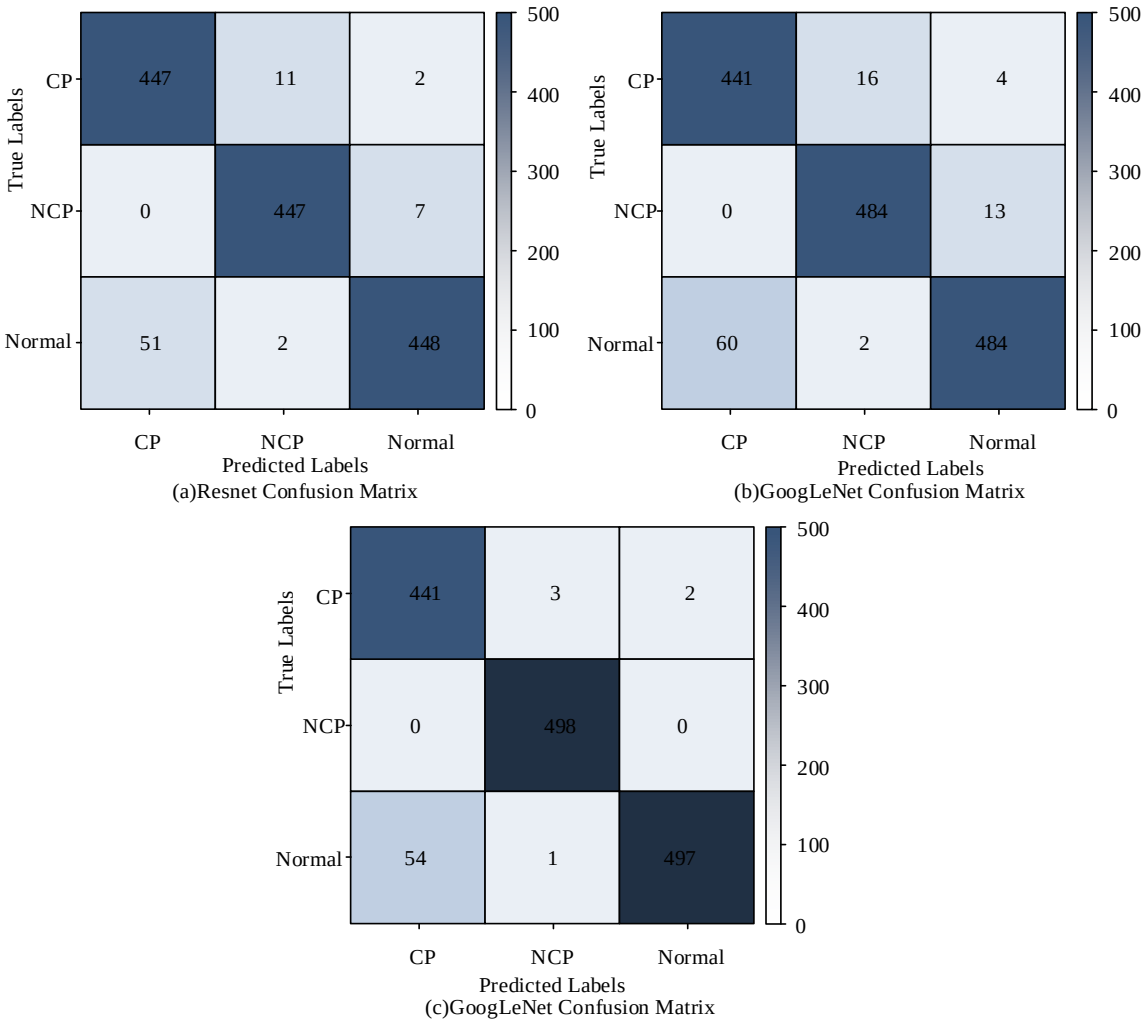

Fig. 11. Comparative analysis of confusion matrix.

Fig. 11(a) shows the confusion matrix of the ResNet model. The accuracy rate of non-severe viral classification is 89.7%. The accuracy rate in classifying abnormal pneumonia images reaches 96.3%. Fig. 11(b) shows the confusion matrix of the Google Net model. It can be seen that the classification accuracy of viral pneumonia using the Google Net model is 88.1%. The accuracy rate of classifying abnormal pneumonia is 88.7%. The classification accuracy of viral pneumonia using the Inception-ResNet model is 98.1%. The accuracy rate of classifying abnormal pneumonia is 98.7%. This method has higher classification accuracy than the other two models for pneumonia images. Compared to other convolutional neural network models, the Inception-ResNet model has higher accuracy, faster processing speed for image classification, and more mature image segmentation technology. In the performance analysis of the system model, the Inception-ResNet model exhibits a zero error rate and extremely high sensitivity. When compared with algorithms such as ResNet and GoogLeNct, the Inception-ResNet algorithm has a lower error rate and higher accuracy and specificity.

V. Discussion

In this study, a lung CT image classification algorithm model based on improved Inception network was proposed, and its performance was verified by experiments. The experimental results show that in CP, the recall rate of Inception-ResNet is 0.953, while that of ResNet and GoogLeNet are 0.812 and 0.701, respectively. In Normal, the recall rate of Inception-ResNet was also about 0.121 and 0.213 higher than the other two algorithms. This result is similar to that of Nigudgi et al. [22]. The results show that the epigenetic-RESnet algorithm has higher accuracy in identifying various types of lung CT images, which is mainly due to the advantages of integrating Inception and ResNet modules to improve the diversity and accuracy of feature extraction. In addition, from the comparison of error rate and specificity, the error rate of the initiation-Resnet algorithm in CP, NCP and Normal is lower than that of the ResNet and GoogLeNet algorithms, and the specificity is significantly higher than the other two algorithms. Especially in CP, the Inception-ResNet error rate is only 0.013%, while the specificity is as high as 90.1%, which is about 31% and 42% higher than ResNet and GoogLeNet, respectively. This

suggests that the Inception-ResNet algorithm performs better in reducing misjudgments and improving classification specificity, which helps to improve the accuracy of lung disease diagnosis.

In addition, the study is compared with CNN, FCN and GraphCut classification algorithms. The results show that the Inception-ResNet algorithm is superior to other algorithms in Dice coefficient, Jaccard coefficient and precision, especially in segmentation accuracy. This result coincides with the conclusion obtained by Sethy team [23]. This further proves the effectiveness of the Inception-ResNet algorithm in lung CT image classification. In terms of model performance analysis, the loss function of the improved Inception model rapidly converges during training and reaches the minimum value within a few iterations, which indicates that the model has high learning efficiency and stability. At the same time, in the image segmentation experiment, the improved U-Net network can segment the lesions with pneumonia characteristics more accurately, which helps doctors to judge the disease more accurately. This study further proves that the Inception-ResNet model can effectively improve the accuracy and efficiency of pulmonary CT image classification by integrating Inception and ResNet modules. In the future, the combination of more medical data and 3D imaging technology is expected to further improve the generalization ability and diagnostic accuracy of the model, and provide more powerful technical support for clinical lung disease diagnosis.

VI. Conclusion

To solve the complex images, small sample data, and similar symptoms between diseases in traditional lung CT medical image processing, the improved Inception algorithm is integrated with the improved U-Net fully convolutional network. The aim is to construct a lung CT image classification model based on an improved Inception network to improve image processing efficiency and lung disease diagnosis speed. In training, the Inception algorithm is compared and analyzed with other algorithms in terms of performance. The results show that the Inception-ResNet algorithm is approximately 0.121 and 0.213 higher than ResNet and GoogLeNct algorithms, respectively. Among CP, NCP, and Normal, this method has the highest recall rate. In the specificity comparison, the algorithm proposed in this research is 90.1% in CP. In NCP, it is about 29.8% and 36.2% higher than ResNet and GoogLeNct. In Normal, it is about 31.2% and 34.3% higher than ResNet and GoogLeNct. In the comparison of model performance, when it is less than 0.1, the improved Inception model's loss function converges rapidly and reaches a minimum value of around 0.18. When the number of iterations is 20, it approaches 0. The classification accuracy of viral pneumonia using the improved Inception model is 98.1%. The classification accuracy of abnormal pneumonia is 98.7%. In summary, the improved Inception network lung CT image classification model can accurately and efficiently process lung CT image classification, which has high practicality and feasibility. Although this research has achieved some results, the future work still needs to be deepened. On the one hand, it is necessary to continue to optimize the algorithm model and explore higher-dimensional feature extraction methods in the future to further improve the classification accuracy and efficiency. On the other hand, given that the current model is based on 2D images and cannot fully reflect the 3D structure of the lung, future research will focus on applying deep learning technology to the field of 3D imaging in order to achieve more accurate diagnosis of lung diseases. In addition, the dataset needs to be expanded to cover more types of lung diseases in the future to enhance the generalization ability and practicality of the model.

Fundings

The research is supported by: The Scientific Research Project of Department of Education of Hunan Province, Research on brain network based on multi-modal imaging, (No.22C0540).

References

[1] Abdulla A A. Efficient computer-aided diagnosis technique for leukaemia cancer detection. IET Image Processing, 2020, 14(17):178-186.

[2] Kassis R W L. Advances in Diagnosis of Progressive Pulmonary and Disseminated Coccidioidomycosis. Clinical infectious diseases, 2021, 72(6):62-89.

[3] Wang B, Chen K, Tian X, Yang Y, Zhang X. An Effective Deep Network for Automatic Segmentation of Complex Lung Tumors in CT Images. Medical Physics, 2021(3):334-357.

[4] Tang W, Yang Q, Hu X, Yan W. Deep learning-based linear defects detection system for large-scale photovoltaic plants based on an edge-cloud computing infrastructure. Solar Energy, 2022, 231(3):527-535.

[5] Li W C, Yan Q R, Guan Y Q, Yang S T, Peng C, Fang Z. Deep-learning-based single-photon-counting compressive imaging via jointly trained subpixel convolution sampling. Applied optics, 2020(23):59-83.

[6] Kocks J W H, Cao H, Holzhauer B, Kaplan A, FitzGerald J M, Kostikas K, Mastoridis P. Diagnostic performance of a machine learning algorithm (Asthma/Chronic Obstructive Pulmonary Disease [COPD] Differentiation Classification) tool versus primary care physicians and pulmonologists in asthma, COPD, and asthma/COPD overlap. The Journal of Allergy and Clinical Immunology: In Practice, 2023, 11(5): 1463-1474.

[7] Annamalai B, Saravanan P, Varadharajan I. ABOA-CNN: auction-based optimization algorithm with convolutional neural network for pulmonary disease prediction. Neural Computing and Applications, 2023, 35(10): 7463-7474.

[8] Wobma H, Bachrach R, Farrell J, Chang M H, Day-Lewis M, Dedeoglu F, Henderson L A. Development of a screening algorithm for lung disease in systemic juvenile idiopathic arthritis. ACR Open Rheumatology, 2023, 5(10): 556-562.

[9] Zhang B, Wang J, Chen J, Ling Z, Ren Y, Xiong D, Guo L. Machine learning in chronic obstructive pulmonary disease. Chinese Medical Journal, 2023, 136(5): 536-538.

[10] Cosentino J, Behsaz B, Alipanahi B, McCaw Z R, Hill D, Schwantes-An T H, Hormozdiari, F. Inference of chronic obstructive pulmonary disease with deep learning on raw spirograms identifies new genetic loci and improves risk models. Nature Genetics, 2023, 55(5): 787-795.

[11] Wang J, Chen X, Lu H, Zhang L, Pan J, Bao Y. Feature-shared adaptive-boost deep learning for invasiveness classification of pulmonary subsolid nodules in CT images. Medical Physics, 2020, 47(4):113-147.

[12] Fukushima N, Shimojima N, Ishitate M. Clinical and structural aspects of tracheal stenosis and a novel embryological hypothesis of left pulmonary artery sling. Pediatric Pulmonology, 2020, 55(3):231-249.

[13] Aggarwal T, Eskandari A, Priya S. Pulmonary embolism rule out: Positivity and factors affec ting the yield of CT angiography. Postgraduate Medical Journal, 2020, 96(11):1130-1156.

[14] Ozawa Y, Shibamoto Y, Hiroshima M, Nakagawa M, Kitase M. Preoperative CT Findings for Predicting Acute Exacerbation of Interstitial Pneumonia After Lung Cancer Surgery: A Multicenter Case-Control Study. American Journal of Roentgenology, 2021, 217(4);119-134.

[15] Lee C H, Jwo J S. Automatic segmentation for pulmonary nodules in CT images based on multifractal analysis. IET Image Processing, 2020, 14(7):1347-1353.

[16] Fang Y, Luo B, Zhao T, He D, Jiang B, Liu Q. ST-SIGMA: Spatio-temporal semantics and interaction graph aggregation for multi-agent perception and trajectory forecasting. CAAI Transactions on Intelligence Technology, 2022, 7(4):744-757.

[17] Zhou L, Mao Q, Huang X, Zhang, F, Zhang Z. Feature refinement: An expression-specific feature learning and fusion method for micro-expression recognition. Pattern Recognition, 2022, 122(2):134-157.

[18] Tarsitano F, Bruderer C, Schawinski K. Image feature extraction and galaxy classification: a novel and efficient approach with automated machine learning. Monthly Notices of the Royal Astronomical Society, 2022, 511(3):3330-3338.

[19] Torre C, Guerreiro J, Longo P, Raposo J F, Leufkens H, Martins A. Intensive monitoring of adverse drug events associated with the use of new glucose-lowering drugs: results from an inception cohort study in Portugal. Diabetic Medicine, 2020, 37(4):116-179.

[20] Guo X L C. The formation of the steady and unsteady air-entrained vortices in pump sump. International Journal of Multiphase Flow, 2020, 129(1):126-137.

[21] Nimrah S, Saifullah S. Context-Free Word Importance Scores for Attacking Neural Networks. Journal of Computational and Cognitive Engineering, 2022, 1(4): 187-192.

[22] Nigudgi S, Bhyri C. RETRACTED ARTICLE: Lung cancer CT image classification using hybrid-SVM transfer learning approach. Soft Computing, 2023, 27(14): 9845-9859.

[23] Sethy P K, Geetha Devi A, Padhan B, Behera S K, Sreedhar S, Das K. Lung cancer histopathological image classification using wavelets and AlexNet. Journal of X-Ray Science and Technology, 2023, 31(1): 211-221.